RSC Advances

ROYAL SOCIETY OF CHEMISTRY

www.rsc.org/advances

Journal Name

ARTICLE

Performance and characteristics of fluoride adsorption using Nanomagnetite graphite-La adsorbent

Shuangxi Wen, Yili Wang* and Shuoxun Dong

Received 00th January 20xx,
Accepted 00th January 20xx

DOI: 10.1039/x0xx00000x

www.rsc.org/

Excessive fluoride in water can cause a series of health problems. In this study, a three-element adsorbent (γ-Fe_2O_3-graphite-La, MGLNP) was successfully developed for fluoride adsorption. Magnetic graphite nanoparticles (MGNP) were synthesized through the chemical deposition of Fe_3O_4 nanoparticles onto nanographite powder (NG) under alkaline conditions. The MGLNP was synthesized by immersing the MGNP in a saturated solution of $La(NO_3)_3{\cdot}6H_2O$ and calcining at 300 °C for 3 h in a muffle furnace. These nanoparticles featured a quick and easy separation process with the saturation magnetization of 26.66 emu·g^{-1}. The surface charge of the MGLNP was highly pH-dependent, the corresponding pH_{pzc} was approximately 7.9. The fluoride adsorption isotherm of the MGLNP could be well described by the Langmuir equation, and the maximum adsorption capacity was about 77.12 mg·g^{-1} at 25 °C and pH = 7 ± 0.1. The kinetics of the fluoride adsorption was described by a pseudo first-order rate law. As the pH decreased, the fluoride adsorption capacity of the MGLNP continuously increased. The effects of the co-existing anions indicated that the anions had minimal effect on the fluoride adsorption. After six cycles of reuse, the MGLNP could still maintain 77.54% adsorption capacity. On the basis of the zeta potential analyses, FTIR spectroscopy, and XPS measurements, ion exchange, combination of La^{3+} and F^-, as well as electrostatic attraction could be observed in the fluoride adsorption process.

1. Introduction

Fluoride is a persistent and non-degradable pollutant that accumulates in soil, plants, wildlife, and humans. For many years, fluoride has been used as a raw material in several industries (e.g., electronics), which typically discharge fluoride-containing wastewater to the environment.[1] In low concentrations, fluoride in water is considered an essential micronutrient that prevents dental carries and facilitates the mineralization of hard tissues; whereas in high concentrations, fluoride can be a health hazard.[2] Excess fluoride in groundwater has been recognized as a serious problem worldwide.[3] The long-term intake of water with high fluoride content by both humans and animals can result in the softening of bones, ossification of tendons and ligaments, and abnormal bone growth called skeletal fluorosis. The World Health Organization has set a guidance value of 1.5 mg·L^{-1} for fluoride in drinking water[4] while China has set its standard to 1.0 mg·L^{-1}.

Various technologies, such as ion exchange, precipitation, nanofiltration, electrocoagulation, and adsorption, have been employed to remove fluoride from water.[5] Precipitation and adsorption are the most widely used techniques for defluorination. Precipitation is convenient and cheap, but its dosage requirement is high; moreover, the addition of alkali, calcium, and magnesium increases the alkalinity of the treated water, and the final concentration of fluoride usually exceeds the permissible limit.[6] Adsorption is regarded as one of the most effective, economical, and environmentally friendly defluoridation techniques because of its high selectivity, easy handling, and low operating cost.[7]

For these reasons, several natural, modified, and synthetic adsorbents, such as activated alumina, bone char,[8] Fe–Al–Ce trimetal oxide adsorbent,[9] zeolite,[10] biochar,[11] hydrous zirconium oxide,[12] metal ion-loaded fibrous protein,[13] and Fe-Mg-La,[1] have been employed to remove fluoride ions from water. However, these materials have certain disadvantages, including low adsorption capacity, separation difficulty, narrow available pH range, and poor mechanical strength. Thus, developing an effective adsorbent that features high fluoride removal efficiency and easy separation is necessary.

In recent years, a number of studies have proved that the rare earth element lanthanum (La) loaded on a fluoride adsorbent can increase fluoride adsorption capacity.[14] Cheng et al.[15] reported that a La^{3+}-modified activated alumina adsorbent for the removal of fluoride from water had a significantly higher maximum adsorption capacity (q_{max} = 6.70 mg·g^{-1}) than an activated alumina (q_{max} = 2.7 mg·g^{-1}). Yu et al.[16] proposed an innovative La-modified carbon (LMC) adsorbent rooted in *Sargassum sp.* for fluoride removal; the maximum adsorption capacity of the LMC adsorbent could reach 94.34 mg·g^{-1} at a neutral pH and is thus substantially higher than that of many commercial adsorbent.

In addition, magnetic adsorbent materials have become a famous research focus in recent years. Magnetic carbon materials, such as magnetic-activated carbon nanoparticles[17] and magnetic carbon nanotubes,[18] have been widely developed as adsorbents for separating contaminants from aqueous solutions. Unlike traditional

* Beijing Forestry University, Beijing 100083, People's Republic of China. Phone: +86-10-62336673; Fax: +86-10-62336596; E-mail: wangyilimail@126.com

adsorbents, magnetic adsorbents feature a quick and easy separation process that does not require additional centrifugation or filtration procedures; these adsorbents also avoid time-consuming column passing operations encountered in the traditional solid phase extraction process.[19]

The aim of the present study is to develop and characterize a nanographite (NG)-loaded magnetic γ-Fe_2O_3 nanoparticle and La(III) adsorbent (MGLNP) for the removal of fluoride from drinking water. The characteristics of the adsorbent were analyzed using zeta potential analysis, field emission scanning electron microscopy, vibrating sample magnetometer (VSM), Fourier transform infrared spectroscopy (FTIR), and X-ray photoelectron spectroscopy (XPS). Batch experiments that considered adsorption kinetics, equilibrium, and the effects of initial pH, fluoride concentration, and coexisting anions on fluoride removal were also conducted to evaluate the adsorption performance of the MGLNP adsorbent.

2. Materials and methods

2.1. Materials

The NG material (average granularity, 85 nm; graphite content ≥ 99.9%) was procured from Beijing Nachen Co., Ltd. The analytical grade chemicals, including $FeCl_3{\cdot}6H_2O$, $FeCl_2{\cdot}4H_2O$, $La(NO_3)_3.6H_2O$, NaOH, and NaF, were purchased from Sinopharm Chemical Regent Beijing Co., Ltd. The F^- stock solution was prepared by dissolving 2.2100 g NaF (analytical grade) in 1,000 mL tap water. The solutions of required concentrations used in this study were obtained by diluting given concentrations of stock solution in city water.

2.2. Synthesis of adsorbent

First, graphite was purified with 3 mol·L^{-1} HNO_3 for 6 h under stirring. The purified graphite was chemically activated via sonication in a mixture of concentrated sulfuric acid and nitric acid (3:1) for 3 h at 70 °C. The graphite was then washed with distilled water and dried. Subsequently, 2 g of activated graphite was suspended in 100 mL mixed solution containing $FeCl_3{\cdot}6H_2O$ (4.7030 g) and $FeCl_2{\cdot}4H_2O$ (1.7296 g). When the temperature reached 80 °C, 15 mL ammonia was added into the solution with stirring. The reaction continued for 90 min. The magnetic graphite was magnetically separated and washed repeatedly with deionized water until the pH reached 7. The product was dried at 60 °C for further use.

The dried magnetic graphite was immersed in 200 mL saturated $La(NO_3)_3{\cdot}6H_2O$ solution for 24 h under 160 rpm stirring in an air bath thermostat oscillator. The product was magnetically separated and calcined at 300 °C for 3 h in a muffle furnace. Upon cooling down to room temperature, the product was washed with distilled water thrice. The adsorbent was dried at 60 °C for further use.

2.3. Fluoride adsorption experiments

All the adsorption experiments were carried out in 150 mL polyethylene bottles that were shaken at 160 rpm in the air bath thermostat oscillator. The reaction volume was 100 mL. The adsorbent was fixed at 0.2 g·L^{-1}, and the pH of the solution was adjusted by adding 0.05 mol·L^{-1} HCl or NaOH. After adsorption, the adsorbent was magnetically separated from the solution, and the F^- concentration was analyzed with a fluoride-selective electrode connected to an ion meter (Thermo, Orion 4 star, U.S).

The kinetic study was conducted under 25 °C, 35 °C, and 45 °C and pH 7.0 ± 0.1 at different time intervals with an initial fluoride concentration of 9.88 mg/L. Samples were taken at predetermined times and immediately separated under a magnetic field for the residual F^- measurement.

To further investigate the characteristics of the adsorption kinetics of the MGLNP, the pseudo first-order model, pseudo second-order model and the Elovich equation were used to fit the adsorption kinetics data.[13]

Pseudo first-order model:

$$\log(q_e - q_t) = \log q_e - K_1 t / 2.303 \quad (1)$$

Pseudo second-order model:

$$t/q_t = 1/(K_2 q_e^2) + t/q_e \quad (2)$$

Elovich equation:

$$q_t = \ln(\alpha\beta)/\beta + (\ln t)/\beta \quad (3)$$

where q_e is the equilibrium adsorption capacity (mg·g^{-1}), q_t is the adsorption capacity at time t (min), and K_1 and K_2 are the rate constants of the pseudo first-order model and pseudo-second-order model, respectively.

The apparent adsorption activation energy was calculated with the Arrhenius equation. The Arrhenius equation is given as follows:

$$K = A\exp\frac{E_a}{RT} \quad (4)$$

Taking the logarithm on the both sides forms the following equation:

$$\ln K = -\frac{E_a}{RT} + \ln A \quad (5)$$

where K is the rate constant of adsorption dynamics, R is the universal gas constant (8.314 J·mol^{-1}·K^{-1}), and T is the absolute temperature in Kelvin. The values of E_a can be obtained from the slope and intercept of the linear plot ln$K$ versus 1/T.

Isotherm experiments were carried out with initial F^- concentrations from 1.97 mg·L^{-1} to 244.6 mg·L^{-1} at 25 °C, 35 °C, and 45 °C under pH 7.0 ± 0.1. The F^- absorbed MGLNP was magnetically separated from the solution after the polyethylene vessels were shaken for 24 h, and the residual F^- was analyzed. Moreover, La in the solution was analyzed with the method reported by Dong et al..[20]

To quantify the fluoride adsorption capacity of the adsorbent and to describe the adsorption mechanism, Langmuir, Temkin and Freundlich equations were adopted in defining the fluoride adsorption isotherm of the MGLNP.

The Langmuir equation is given as follows:

$$Q_e = Q_m K_L C_e / (1 + K_L C_e) \quad (6)$$

Temkin equation:

$$Q_e = A + B \log C_e \quad (7)$$

where C_e is the equilibrium concentration (mg·L^{-1}), Q_e is the amount adsorbed under equilibrium (mg·g^{-1}), Q_m is the theoretical maximum adsorption capacity, and K_L (L·mg^{-1}) is a Langmuir constant, which indicates the affinity of F^- toward the adsorbent. A, B are the Temkin constants.

The Freundlich equation, which is indicative of the surface heterogeneity of the adsorbent, is given as follows:

$$Q_e = K_f C_e^{1/n} \quad (8)$$

where K_f and $1/n$ are the Freundlich constants related to adsorption capacity and adsorption intensity (heterogeneity factor), respectively.

To evaluate thermodynamic feasibility and further analyze the nature of the adsorption process, the distribution constant K_0 obtained at the mentioned temperatures was utilized in the computation of the three basic thermodynamic parameters using the following equations:[21]

$$K_0 = \frac{q_e}{C_e} \quad (9)$$

$$\Delta G^\circ = -RT \ln K_0 \quad (10)$$

$$Ln K_0 = -\frac{\Delta H^o}{RT} + \frac{\Delta S^o}{R} \quad (11)$$

where $\Delta G°$ (kJ·mol^{-1}) is the free energy of sorption, K_0 (L·g^{-1}) is the distribution constant, T is the absolute temperature in Kelvin, R is the universal gas constant (8.314 J·mol^{-1}·K^{-1}), $\Delta H°$ is the standard enthalpy entropy change (kJ·mol^{-1}), and $\Delta S°$ is the standard entropy change (J·mol^{-1}·K^{-1}).

The effect of equilibrium pH on F^- adsorption was investigated by adjusting the solution pH to 4.0–10.0 at 25 °C under an initial F^- concentration of 9.88 mg·L^{-1} according to the procedure of the adsorption isotherm experiment.

The effects of co-existing anions (phosphate, arsenate, nitrate, chloride, and sulfate) on fluoride adsorption were investigated by performing fluoride adsorption under a fixed adsorbent dose of 200 mg·L^{-1}, initial fluoride concentration of 9.88 mg·L^{-1} at 25 °C, solution pH of 7.0 ± 0.1, and a series of target anion concentrations. The reproducibility of the results was confirmed by performing all experiments in triplicate.

2.4. Desorption and reuse

Fluoride adsorption was first conducted under a fluoride concentration of 97.7 mg·L^{-1}; the other procedures were the same as those employed in the study on adsorption isotherm. The F^- absorbed MGLNP was collected through magnetic separation and then air-dried for fluoride desorption. This adsorbent was suspended in 50 mL NaOH solutions with different concentrations under 160 rpm shaking in the air bath thermostat oscillator at 25 °C for 12 h. The fluoride concentrations in the desorption solutions were subsequently analyzed.

The defluorinated MGLNP was collected for the experiment by repeating the aforementioned adsorption and desorption procedures. The adsorbents were reused for six cycles in this study.

2.5. Characterization of the adsorbent before and after F^- adsorption

The magnetism characteristics of the adsorbent were observed with a VSM (LakeShore-7407). The zeta potentials of the adsorbent were determined using a zeta potential meter (Zetasizer 2000, Malvern UK). A scanning electron microscope (SEM) (Carl Zeiss-Merlin), coupled with an energy dispersive X-ray spectrometer (EDX) and an X-ray diffraction analyzer (XRD) (BruckerD-8 Diffractometer, Germany), was used to characterize the morphological information of the adsorbent. The functional groups on the surface of the adsorbent and their binding energies were observed via FTIR (Perkin Elmer-Spectrum One) and XPS equipment (ESCA-Lab-5 spectrometer).

3. Results and discussion

3.1 Material characterization

Fig. 1 shows the magnetization curves and zeta potential of the MGLNP. As shown in Fig. 1a, the saturation magnetization of the MGNP was initially 36.18 emu·g^{-1}, which decreased to 26.66 emu·g^{-1} after La was loaded to the magnetic graphite. The latter value proved to be higher than that of magnetic carbon with a saturation magnetization of 24.9 emu.g^{-1}, as reported by Gao et al..[18] As can be seen from the picture in the Fig.1a, the MGLNP was attracted to the wall of the vial with an external magnetic field. This condition differed from the black homogeneous dispersion without an external magnetic field.

Fig. 1. Physical properties of MGNP or MGLNP: (a) magnetization curves; (b) zeta potential vs. pH of MGLNP at 25 °C.

As shown in Fig. 1b, the value of pH_{pzc} of the MGLNP adsorbent was approximately 7.9, which indicated that the surface charge of the adsorbent was highly pH-dependent. When pH > 7.9, the zeta potentials were negative and further decreased as pH increased. This condition produced a strong electrostatic repulsion between the adsorbent and the fluoride anions. By contrast, the surface charge became positive when the solution pH was below pH_{pzc}, which is conducive to the adsorption of fluoride. Compared with other fluoride adsorbents, such as the La-modified carbon (pH_{pzc} = 6.12)[16] and Fe–Al–Ce adsorbent (pH_{pzc} = 7.5),[9] MGLNP has a higher pH_{pzc}, which equates to a wide pH range applicable in fluoride adsorption.

In Supporting Information, the SEM characterization results showed the layered structure of the NG (Fig. S1a). After γ-Fe_2O_3 and La were loaded on the surface of the NG, the adsorbent particles became an amorphous structure comprising small, aggregated particles (Fig. S1c). The size of the MGLNP is shown in Fig. S1c. As revealed by the EDX analysis (Fig. S2), La was successfully immobilized on the surface of the adsorbent, and the atomic ratio of La, Fe, and C in the adsorbent was La:Fe:C=1:1.3:3.3. The XRD spectra (Fig. S3) also show that γ-Fe_2O_3 and La were successfully loaded on the NG.

3.2 Adsorption kinetics

The adsorption kinetics of the MGLNP is illustrated in Fig. 2. The amount of F^- adsorbed by the MGLNP increased rapidly and almost reached equilibrium within 30 min under three different temperatures. Furthermore, the fluoride adsorption capacity increased with temperature.

Fig. 2. Adsorption kinetics of fluoride on MGLNP (initial fluoride concentration = 9.88 mg·L^{-1}, adsorbent dosage = 200 mg·L^{-1}, natural pH, 25 °C).

Three models were used to fit the adsorption kinetic curves in Fig. 2. The kinetic data under the three different temperatures were best fitted by the pseudo first-order adsorption rate model. The corresponding model parameters are provided in Tab. 1. K_1 increased with temperature. A large K_1 value usually indicates a fast adsorption rate.[16] The theoretical and experimental q_e values agreed well, implying that the fluoride adsorbed on the MGLNP underwent chemical adsorption, with the adsorption mechanism being the rate-controlling step.[22] The apparent adsorption activation energy E_a = 19.73 kJ·mol^{-1}. This result indicated that the adsorption process occurred because of chemisorptions.[23]

Tab. 1. Adsorption kinetics Parameters of Fluoride adsorption on MGLNP.

3.3 Adsorption isotherm

The fluoride adsorption isotherms of the MGLNP at different temperatures are shown in Fig. 3. At three different temperatures, the adsorption capacity increased rapidly when F^- was less than 100 mg·L^{-1}. When F^- concentration was higher than 100 mg·L^{-1}, the adsorption capacity increased gradually and reached equilibrium. Moreover, adsorption capacity increased with temperature.

Fig. 3. Fluoride adsorption isotherm at different temperatures (adsorbent dosage = 200 mg·L^{-1}, pH=7 ± 0.1, equilibrium time: 24 h).

The Freundlich, Langmuir and Temkin models were fit to describe the experimental adsorption results. The Langmuir parameters Q_m and K_L were calculated from the slope and intercept of the linear plots of $1/Q_e$ versus $1/C_e$. The values of the Freundlich parameters K_f and 1/n were obtained from the slope and intercept of the linear Freundlich plot of $\log Q_e$ versus $\log C_e$. The corresponding determination coefficients (R^2) are presented in Tab. 2.

Tab. 2. Adsorption isotherm Parameters of Fluoride adsorption on MGLNP.

In terms of the determination coefficients (R^2), the Langmuir equation is more suitable to describe adsorption behavior than the Freundlich model. The maximal adsorption capacities for fluoride calculated with the Langmuir model were 77.12, 87.27, and 100.90 mg·g^{-1} at 25 °C, 35 °C, and 45 °C, respectively. The concentration of La in the solution after fluoride adsorption was 0.12 mg·L^{-1}, which was much lower than 0.79 mg·L^{-1} reported by Li et al.[24]

According to the K_L values at different temperatures, the thermodynamic parameters were determined with Eqs. (9)–(11). The results are shown in Tab. 3.

Tab. 3. Thermodynamic Parameters of Fluoride adsorption on MGLNP.

A negative $\Delta G°$ confirmed the feasibility and spontaneous nature of the fluoride adsorption.[13] The $\Delta G°$ value became increasingly negative as the temperature rose, thus indicating that the extent of spontaneity is proportional to temperature and that a high temperature facilitates the adsorption process.[21] The temperature-dependent $\Delta H°$ value was 21.13 kJ·mol^{-1}. The positive $\Delta H°$ indicated the endothermic nature of the adsorption process[25] and confirmed that the intensity of the adsorption process was enhanced at high temperatures.[21] The positive $\Delta S°$ indicated the affinity of the adsorbent to fluoride ions and suggested an increased randomness at the solid/solution interface during the adsorption of fluoride ions onto the MGLNP. These findings may be related to the release of water of hydration during the adsorption process, which increased the randomness of the system.[25]

3.4 Effects of pH on fluoride adsorption

The effect of solution pH on fluoride adsorption is presented in Fig. 4. Fluoride adsorption was highly pH-dependent, and adsorption capacity decreased as pH increased.

Fig. 4. Effect of aqueous phase pH on the fluoride adsorption of MGLNP (initial fluoride concentration = 9.88 mg·L^{-1}, adsorbent dosage =200 mg·L^{-1}, 25 °C).

The drop in fluoride removal efficiency vs. pH may be explained as follows. The hydroxyl ions in a solution gradually increase with solution pH value,[26] and hydroxyl ions have a similar ion radii with fluoride ions. Furthermore, it was found that the final pH of the solution was significantly higher than the initial pH, thus indicating that a number of hydroxide ions were released into the solution.[14] Hence, the inhibition of fluoride adsorption mainly resulted from the competition for surface adsorption sites because of increasing hydroxyl ions. The changes in the pH-dependent electrostatic force existing between the adsorbent surface and fluoride also affected fluorine adsorption efficiency. A low pH favors the protonation of adsorbent surfaces. Enhanced protonation generates a high number of positively charged sites per unit surface area (Fig. 1b). This condition increases the electrostatic attraction force between a positively charged surface and negative fluoride ions, thus increasing the amount of adsorption at low pH values.[12] In an acidic pH range (pH < 5), weak hydrofluoric acid is present in the solution; as pH increases, the fluoride with F^- as the main existing form may affect defluoridation.[27]

3.5 Effects of coexisting anions on fluoride adsorption

Considering that some anions commonly exist in actual

groundwater, the effects of sulfate, chloride, nitrate, and carbonate on the fluoride adsorption of the MGLNP adsorbent were examined. The results are given in Fig. 5.

Fig. 5. Effect of coexisting anions on fluoride adsorption of MGLNP (initial fluoride concentration = 9.88 mg·L^{-1}, adsorbent dosage = 200 mg·L^{-1}, natural pH, 25 °C).

As presented in Fig. 5, sulfate and chloride did not significantly interfere with the fluoride removal process even at a concentration of 100 mg·L^{-1}, whereas nitrate and carbonate showed adverse effects when the concentration reached 100 mg·L^{-1}. When the concentration of these anions was at 100 mg·L^{-1}, nitrate significantly reduced the fluoride adsorption among the anions on the MGLNP. Fluoride adsorption decreased from 18.27 mg·g^{-1} to 11.33 mg·g^{-1} as nitrate concentration increased from 0 mg·L^{-1} to 100 mg·L^{-1}. The effects followed the decreasing order NO_3^- > CO_3^{2-} > SO_4^{2-} > Cl^-.

3.6 Desorption, reuse and stability

Loaded adsorbent must feature high adsorption capacity, offer reclaim convenience, and facilitate desorption. Adsorbents should maintain a considerable adsorption capacity after several uses. A NaOH solution was selected as the desorption reagent because its effectiveness has been proved by previous studies.[9] The desorption of fluoride from the loaded MGLNP adsorbent under different NaOH concentrations and the reuse effect of the MGLNP adsorbent were investigated. The results are presented in Fig. 6.

Fig. 6. Desorption and reuse. (a) Desorption of fluoride from loaded MGLNP adsorbent under different pH values, loaded adsorbent: 0.02 g, equilibrium time: 12 h, 25 °C; (b) regeneration results of MGLNP in six cycles.

As presented in Fig. 6a, a small amount of fluoride was released from the loaded adsorbent at a pH lower than 11.0. However, desorption efficiencies were 95.85% and 97.42% when the pH was increased to 12.0 and 13.0 (corresponding to NaOH concentrations of 0.4 and 4.0 g·L^{-1}, respectively), respectively. Considering the dosage of NaOH, pH = 12.5 was selected for the desorption of fluoride in the reuse experiment. The MGLNP adsorbent performed well after reuse (Fig. 6b). It maintained an adsorption capacity of 77.54% at the sixth cycle of fluoride adsorption.

In supporting information, the cost analysis of MGLNP adsorbent and comparison with other adsorbents were presented in Tab. S1 and Tab.S2, respectively. The results indicated that MGLNP adsorbent had a potential for fluoride removal from drinking water.

The stability experiments of MGLNP were carried out according to the procedure in section 4 of the supporting information. Fig. S4 and Tab. S3 show that MGLNP had a stable performance in terms of magnetic separation and fluoride adsorption capacity when it was treated for 8 days with different pH values or temperatures.

3.7 Adsorption mechanism

3.7.1 FTIR

The FTIR spectra of the adsorbents before and after fluoride adsorption are compared in Fig. 7. As illustrated, the absorption bands of the Fe-O bond were 558 and 560 cm^{-1}, which indicated that γ-Fe_2O_3 combined with graphite.[28] The sharp peaks at approximately 635 cm^{-1} could be attributed to the stretching vibration of the La–O bond.[29] Several significant bands in the virgin adsorbent could be attributed to the carboxylic acid groups introduced by the acid oxidizing process of the graphite, as well as by the appearance of the peak at 1,434 cm^{-1}, which corresponded to the –COOH and O–H stretching bands at 3,422 cm^{-1}.[30] The peaks at 1,384 cm^{-1} were attributed to the in-plane bending vibration of methyl (–CH_3).[18] The peaks at 859 and 1,489 cm^{-1} confirmed the presence of a CO_3^{2-} group.[27]

Fig. 7. FTIR spectra of the adsorbents.

After fluoride removal, the peaks at 1,384 cm^{-1} almost disappeared; the peaks at 1,434 and 1,489 cm^{-1} became very weak and shifted to 1,436 and 1,473 cm^{-1}, respectively, thus indicating that an interaction occurred between the adsorbents and fluoride during the adsorption process.[31] Hence the –COOH and carbonate groups were partly lost after fluoride adsorption.[26] In addition, the peak area at 3,422 cm^{-1} (assigned to –OH) decreased after adsorption, thus indicating that the hydroxyl on the adsorbent participated in the fluoride adsorption process. Therefore, the surface ion exchange process based on –COOH, carbonate ions (CO_3^{2-}), and surface hydroxyl ions (OH^-) exchanged with F^- may occur in the fluoride removal process.

3.7.2 XPS spectroscopy

To explore the fluoride adsorption mechanism of the MGLPNs, the adsorbents before and after fluoride adsorption were analyzed using XPS. As shown in Fig. 8, the wide scan XPS spectrum of the virgin adsorbent indicated that Fe, La, C, and O existed in the adsorbent. Meanwhile, a fluoride characteristic peak at 685.2 eV was observed in the XPS spectrum of the adsorbent after fluoride adsorption, thus indicating that fluoride was successfully adsorbed.[32] The intensity of O 1s significantly decreased after fluoride adsorption.

Fig. 8. XPS wide scan spectra of the adsorbents: (A) virgin adsorbent (B) F^- loaded adsorbent.

A high-resolution scan of the O 1s spectrum of the fresh adsorbent is shown in Fig. 9a. The scan can be divided into three component peaks at 530.50, 532.04, and 533.44 eV, which can be assigned to metal oxide (M–O), hydroxyl group bonded to metal (M–OH), and carbonate group (C–O) in the adsorbent,[16] respectively. As shown in Tab. 4, after fluoride adsorption, the relative area ratio for the peak could be attributed to the increase of M–O from 27.25% to 38.41%. By contrast, the relative areas for the peaks attributed to M–OH and C–O decreased from 41.62% to 33.37% and from 31.13% to 28.22%, respectively. The decreases suggested the participation of the O–H group in the fluoride adsorption process through the ion exchange process. The same result was achieved in the FTIR analysis.

Fig. 9. XPS spectra of the O 1s of the adsorbents: (a) before adsorption; (b) after adsorption.

Tab. 4. Deconvolution of XPS O 1s spectra for the MGLNP sample before and after fluoride adsorption from a 50 $mg \cdot L^{-1}$ aqueous solution.

On the basis of the comprehensive analysis of the FTIR and XPS results, the possible mechanism for the fluoride removal of the MGLNP could be conjectured as the surface ion exchange process based on –COOH, carbonate ions (CO_3^{2-}), and surface hydroxyl ions (OH^-) exchanged with F^- and the combination of La^{3+} and F^-, as described in Fig. 10.

Fig. 10. Illustration of the possible mechanism of the fluoride adsorption of MGLNP.

Moreover, the fluoride removal data were estimated through quantitatively calculating the [OH^-] increase and the loaded La^{3+} on the surface of MGLNP. The corresponding results were shown in Tab. S4, which implied that surface La^{3+} complexation mechanism played an important role in the fluoride removal by MGLNP.

4. Conclusions

In this study, a three-element adsorbent (γ-Fe_2O_3-graphite-La) was successfully developed for fluoride adsorption. The maximum adsorption capacity was approximately 77.12 $mg \cdot g^{-1}$ at 25 °C and pH = 7 ± 0.1. The kinetic studies showed that the fluoride adsorption followed a pseudo first-order rate law. The zeta potential analyses, FTIR spectroscopy, and XPS measurements proved that the fluoride removal by this adsorbent was the result of the surface ion exchange process based on –COOH, carbonate ions (CO_3^{2-}), and surface hydroxyl ions (OH^-) exchanged with F^- and the electrostatic interaction between the charging surface and fluoride. Moreover, the combination of La^{3+} and F^- performed an important function in the fluoride removal process. The effects of the co-existing anions showed that the anions had minimal effect on the adsorption of fluoride. The reuse experiment indicated that a 77.54% adsorption capacity could be maintained when the adsorbent was used for the adsorption of fluoride up to the sixth cycle. These results highlight the great potential of the adsorbent MGLNP to be used as a material for the removal of fluoride from drinking water.

Acknowledgements

This work was supported by the National Natural Science Foundation of China (Nos. 51478041, 21177010 and 51078035), Major projects on control and rectification of water body pollution (2012ZX07105-002-03).

Notes and references

1 Y. Yu, L. Yu and J. P. Chen, Chemical Engineering Journal, 2015, 262, 839–846.
2 T. Zhang, Q. Li, Z. Mei, H. Xiao, H. Lu and Y. Zhou, Desalin Water Treat, 2014, 52, 3367–3376.
3 M. Amini, K. Mueller and K.C. Abbaspour, Environ. Sci Technol., 2008, 42, 3662–3668.
4 WHO (World Health Organization), Guidelines for Drinking-water Quality, 4th ed., Gutenberg, Malta, 2011.
5 A. Teutli-Sequeira, V. Martínez-Miranda, M. Solache-Ríos, I. Linares-Hernández, Journal of Fluorine Chemistry, 2013, 148, 6-13.
6 E. Oguz, Journal of Hazardous Materials, 2005, 117, 227–233.
7 B. Kemer, D. Ozdes, A. Gundogdu, B. Bulut, V. Duran and V. Soylak, Journal of Hazardous Materials, 2009, 168, 888–894.
8 N.A. Medellin-Castillo, R. Leyva-Ramos, R. Ocampo-Perez, R.F Garcia de la Cruz, A. Aragon-Pina, J.M. Martinez-Rosales, R.M Guerrero-Coronado and L. Fuentes-Rubio, Ind. Eng. Chem Res., 2007, 46, 9205–9212.
9 X. M. Wu, Y. Zhang, X. M. Dou and M. Yang, Chemosphere, 2007, 69, 1758–1764.
10 Y. Sun, Q. Fang, J. Dong, X. Cheng and J. Xu, Desalination 2011, 277, 121–127.
11 D. Mohan, R. Sharma, V.K. Singh, P. Steele and C.U. Pittman Ind. Eng. Chem. Res., 2011, 51, 900–914.
12 X.M. Dou, D. Mohan, C.U. Jr. Pittman and S. Yang, Chemical Engineering Journal, 2012, 198-199, 236–245.
13 H. Deng and X.L. Yu, Ind. Eng. Chem. Res., 2012, 51, 2419–2427.
14 J. Wang, D.J. Kang, X.L. Yu, M.F. Ge and Y.T. Chen, Chemical Engineering Journal, 2015, 264, 506–513.
15 J.M. Cheng, X.G. Meng, C.Y Jing and J.M. Hao, Journal of Hazardous Materials, 2014, 278, 343–349.
16 Y. Yu, C.H Wang, X. Guo and J.P. Chen, Journal of Colloid and Interface Science, 2015, 441, 113–120.
17 B. Kakavandi, A.J. Jafari, R.R. Kalantary, S. Nasseri, A. Ameri and A. Esrafily, Iranian Journal of Environmental Health Sciences & Engineering, 2013, 10, 10–19.
18 L. Gao and L.G. Chen, Microchim Acta, 2013, 180, 423–430.
19 Q. Wu, M. Liu, X. Ma, W. Wang, C. Wang, X. Zang and Z. Wang, Microchim Acta, 2012, 177, 23–30.
20 Y.J. Dong, K. Gai and X.X. Gong, Journal of Chongqing Normal University (Natural Science Edition), 2004, 21, 43-45. (In Chinese)
21 A.R. Sani, A.H. Bandegharaei, S.H. Hosseini, K. Kharghani, H Zarei and A.b Rastegar, Journal of Hazardous Materials, 2015 286, 152–163.
22 X.P. Liao, Y. Ding, B. Wang and B. Shi, Ind. Eng. Chem. Res 2006, 45, 3897–3902.
23 Z. Aksu, Process Biochemistry, 2002, 38, 89–99.
24 Y.F. Li, F.P. Meng and X.P. Du, Materials Review, 2012, 26, 7-9. (In Chinese)
25 N. Chen, C.P. Feng, Z.Y. Zhang, R.P. Liu, Ya Gao, M. Li and N. Sugiura, Journal of the Taiwan Institute of Chemical Engineers,, 2012, 43, 783–789.
26 S. Dey, S. Goswami and U.C. Ghesh, Water Air and Soil Pollution , 2004, 158, 311-323.

27 K.S. Zhang, S.B. Wu, X.L. Wang, J.Y. He, B. Sun, Y. Jia, T. Luo, F. Meng, Z. Jin, D.Y. Lin, W. Shen, L.T. Kong and J.H. Liu, Journal of Colloid and Interface Science,2015, 446, 194–202.
28 J. Li, X.Y. Qiu and Y.Q. Lin, Applied Surface Science, 2010, 256, 6977-6981.
29 M. Ghiasi and A. Malekzadeh, Superlattices and Microstructures, 2015, 77, 295–304.
30 D.L. Xiao, P. Dramou, H. He, L.A. Pham-Huy, H. Li, Y.Y. Yao and C. Pham-Huy, J Nanopart Res, 2012, 14, 984–996.
31 F. Xie, J. Borowiec and J. Zhang, Chemical Engineering Journal, 2013, 223, 584–591.
32 X. Yu, S. Tong, M. Ge and J. Zuo, Carbohydr. Polym., 2013, 92, 269–275.

Journal Name

ARTICLE

Tables

Tab. 1. Adsorption kinetics Parameters of Fluoride adsorption on MGLNP

Temperature (°C)	Pseudo-first-order				Pseudo-second-order				Elovich		
	$q_{e,exp}$ (mg·g^{-1})	$q_{e,cal}$ (mg·g^{-1})	K_1 (min^{-1})	R^2	$q_{e,cal}$ (mg·g^{-1})	K_2 (L·mg^{-1}·min^{-1})	R^2	α (mg·g^{-1}·min^{-1})	β (g·mg^{-1})	R^2
25	17.63	16.83	0.32	0.99	16.59	0.035	0.94	14.58	0.33	0.97
35	20.50	20.34	0.41	0.99	20.08	0.050	0.95	24.07	0.29	0.91
45	24.07	22.29	0.53	1.00	22.84	0.083	0.97	24684.77	0.59	0.70

Tab. 2. Adsorption isotherm Parameters of Fluoride adsorption on MGLNP

Temperature (°C)	Langmuir				Freundlich			Temkin		
	$Q_{e,exp}$ (mg·g^{-1})	Q_m (mg·g^{-1})	K_L (L·mg^{-1})	R^2	1/n	K_f (L·mg^{-1})	R^2	A	B	R^2
25	72.33	77.12	0.038	0.99	0.49	6.29	0.95	-0.38	29.72	0.97
35	79.00	87.27	0.041	0.99	0.47	8.04	0.96	2.50	32.51	0.96
45	94.67	100.90	0.045	0.99	0.46	10.00	0.96	5.76	36.84	0.97

Tab. 3. Thermodynamic Parameters of Fluoride adsorption on MGLNP

Temperature (°C)	$\Delta G°$ (kJ·mol^{-1})	$\Delta H°$ (kJ·mol^{-1})	$\Delta S°$ (J·mol^{-1}K^{-1})
25	-2.53		
35	-3.24	21.13	79.34
45	-4.12		

Tab. 4. Deconvolution of XPS O 1s spectra for the MGLNP sample before and after fluoride adsorption from a 50 mg·L^{-1} aqueous solution.

Sample	Peak	B.E.[a] (eV)	FWHM[b] (eV)	G:L[c] ratio	Percent[d] (%)
Before adsorption	M–O	530.50	1.42	30:70	27.25
	O–H	532.04	1.73	30:70	41.62
	C–O	533.44	2.03	30:70	31.13
After adsorption	M–O	530.43	1.53	30:70	38.41
	O–H	532.12	1.38	30:70	33.37
	C–O	533.32	2.35	30:70	28.22

[a]Binding energy (B.E.); [b]Full width at half maximum (FWHM); [c]Gaussian:Lorentzian ratio; [d]The percentage represents the contribution of each peak to the total number of counts under the O 1s peak.

Figures

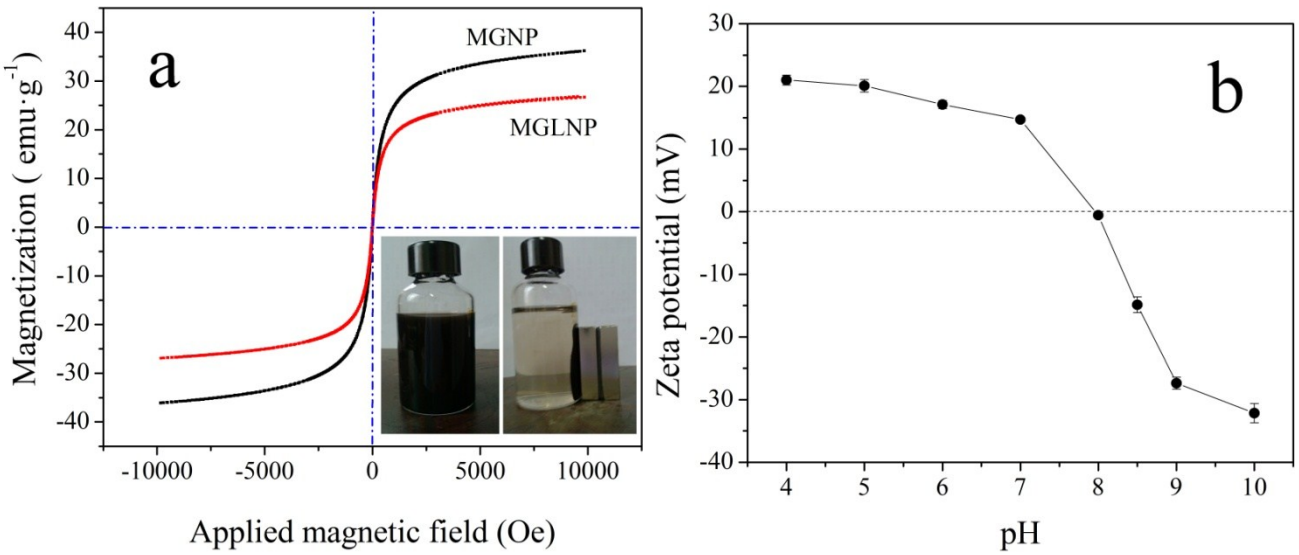

Fig. 1. Physical properties of MGNP or MGLNP: (a) magnetization curves; (b) zeta potential vs. pH of MGLNP at 25 °C.

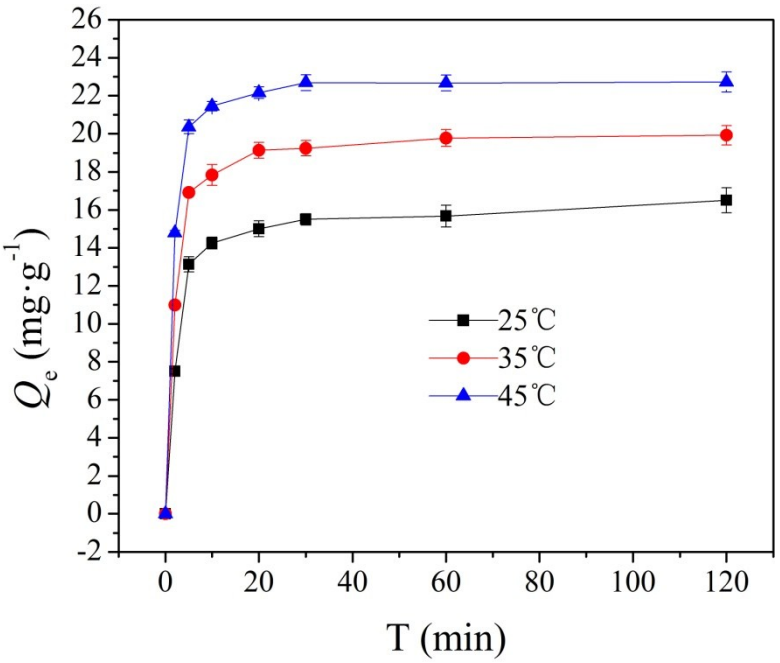

Fig. 2. Adsorption kinetics of fluoride on MGLNP (initial fluoride concentration = 9.88 mg·L^{-1}, adsorbent dosage = 200 mg·L^{-1}, natural pH, 25 °C).

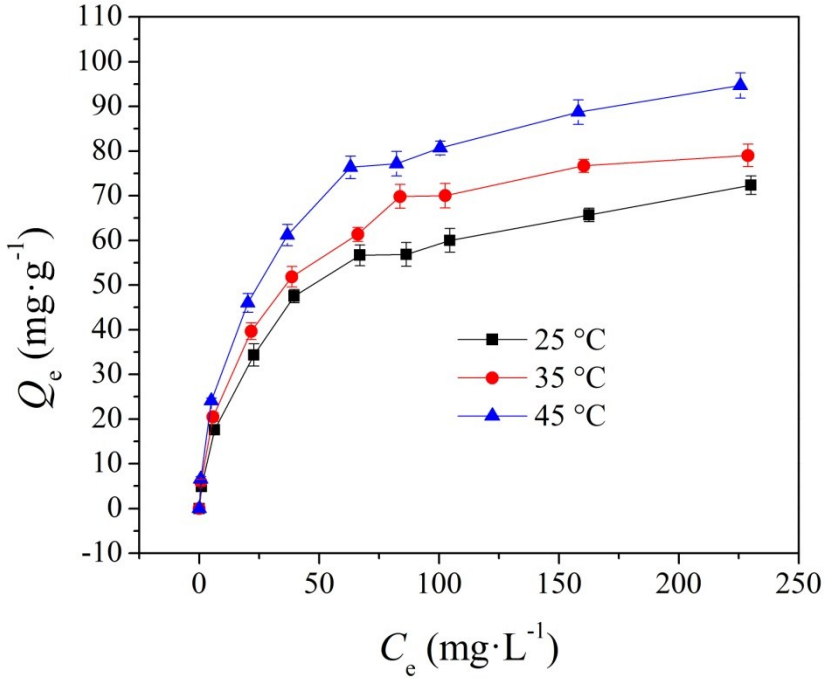

Fig. 3. Fluoride adsorption isotherm at different temperatures (adsorbent dosage = 200 mg·L^{-1}, pH = 7 ± 0.1, equilibrium time: 24 h).

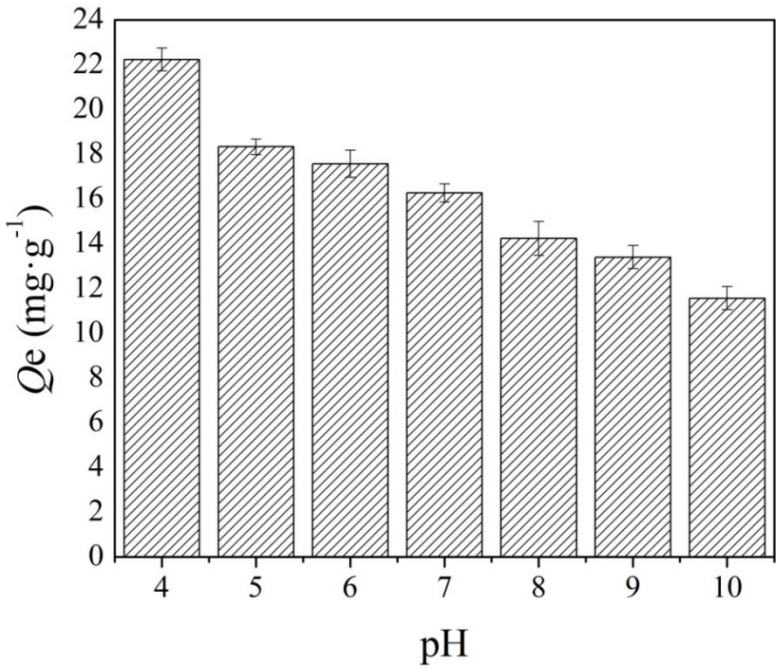

Fig. 4. Effect of aqueous phase pH on the fluoride adsorption of MGLNP (initial fluoride concentration = 9.88 $mg \cdot L^{-1}$, adsorbent dosage = 200 $mg \cdot L^{-1}$, 25 °C).

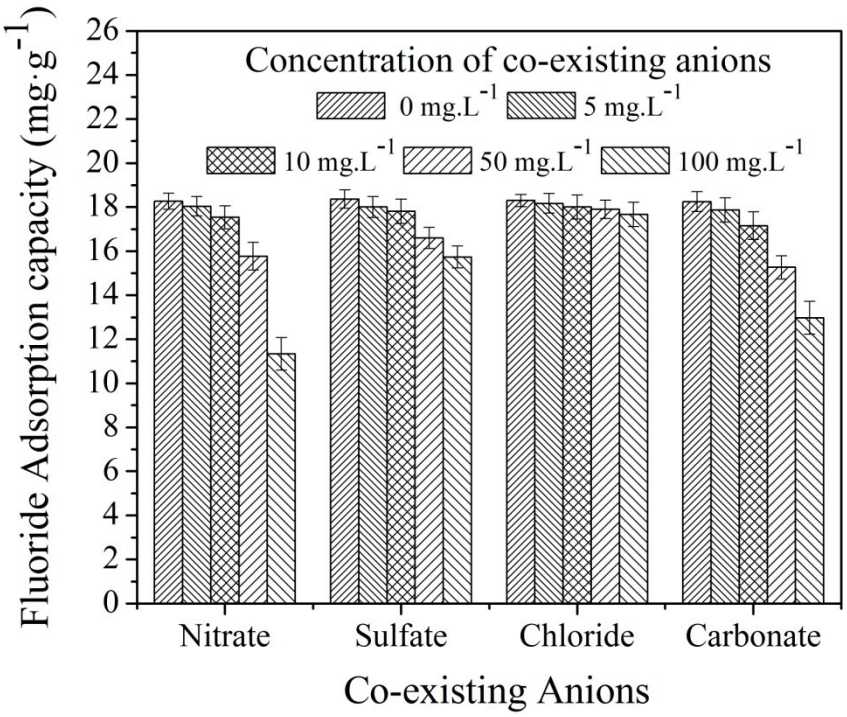

Fig. 5. Effect of coexisting anions on fluoride adsorption of MGLNP (initial fluoride concentration = 9.88 mg·L^{-1}, adsorbent dosage = 200 mg·L^{-1}, natural pH, 25 °C).

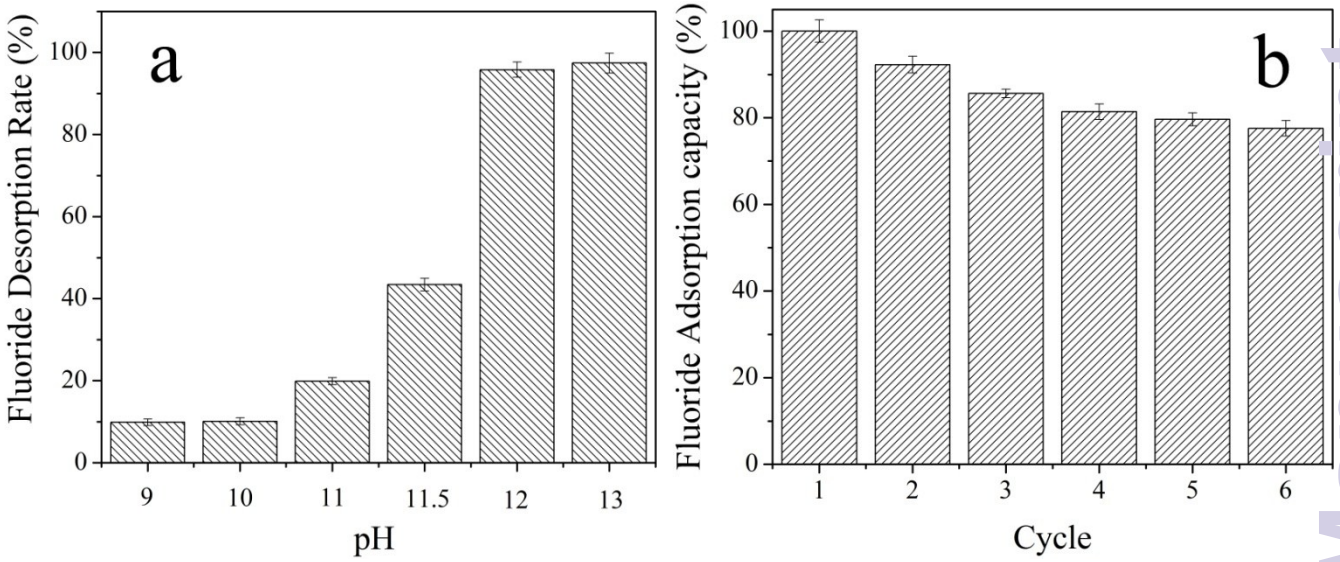

Fig. 6. Desorption and reuse. (a) Desorption of fluoride from loaded MGLNP adsorbent under different pH values, loaded adsorbent: 0.02 g, equilibrium time: 12 h, 25 °C; (b) regeneration results of MGLNP in six cycles.

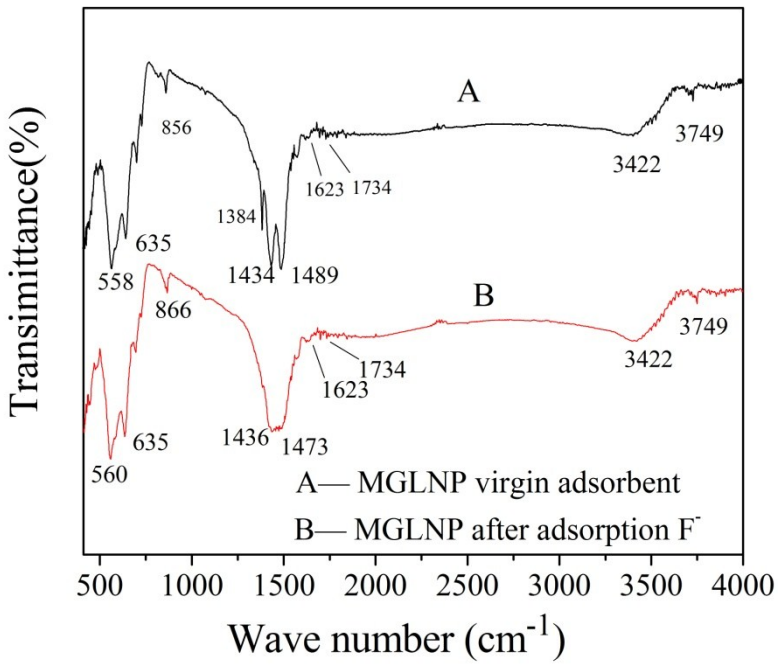

Fig. 7. FTIR spectra of the adsorbents.

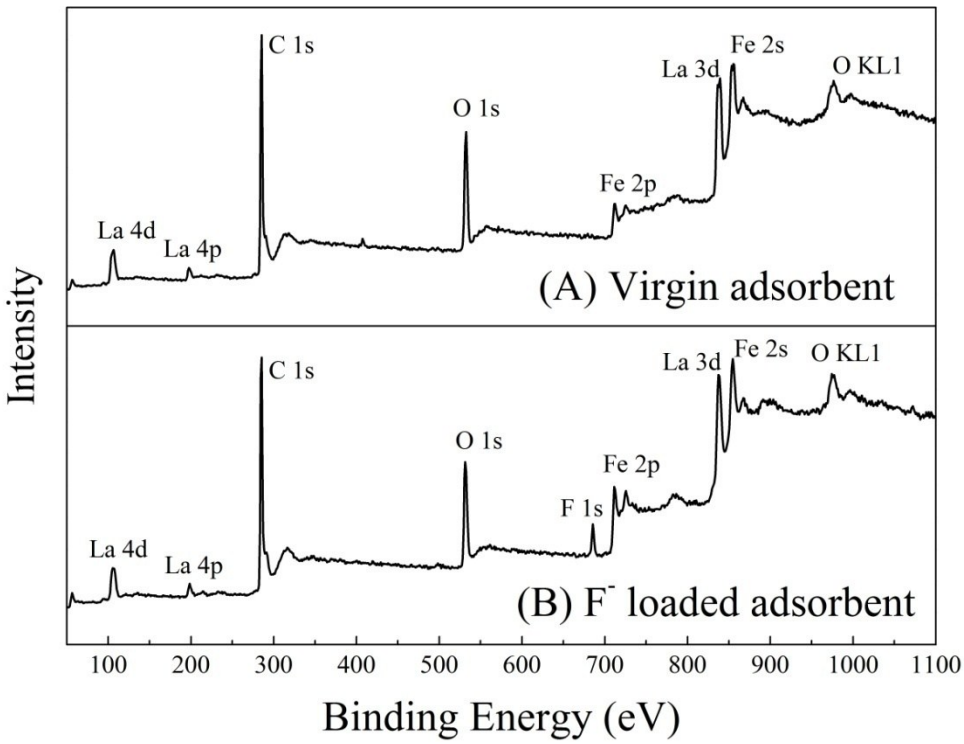

Fig. 8. XPS wide scan spectra of the adsorbents: (A) virgin adsorbent; (B) F^- loaded adsorbent.

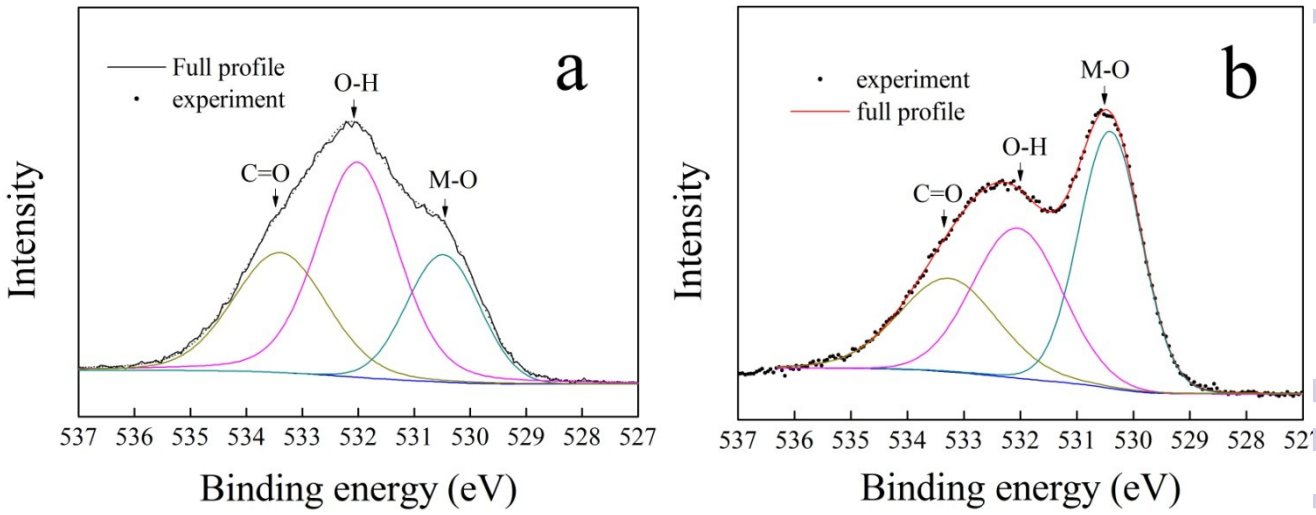

Fig. 9. XPS spectra of the O 1s of the adsorbents: (a) before adsorption; (b) after adsorption.

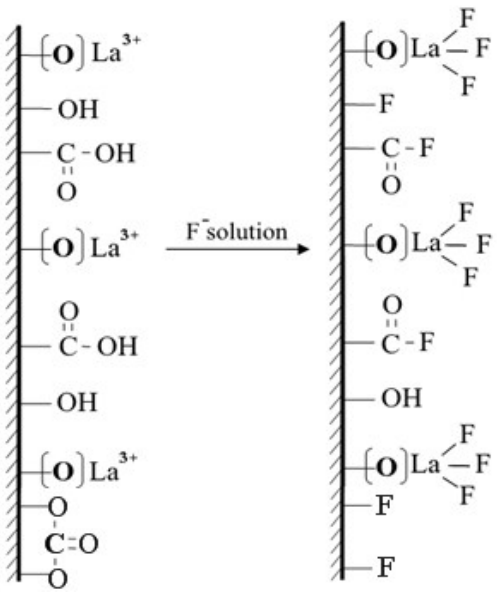

Fig. 10. Illustration of the possible mechanism of the fluoride adsorption of MGLNP.